MNRAS **000**, 1–10 (0000) Preprint 3 April 2022 Compiled using MNRAS LATEX style file v3.0

Four bright eclipsing binaries with γ Doradus pulsating components: CM Lac, MZ Lac, RX Dra and V2077 Cyg

John Southworth [1], Timothy Van Reeth [2]
[1] *Astrophysics Group, Keele University, Staffordshire, ST5 5BG, UK*
[2] *Institute of Astronomy, KU Leuven, Celestijnenlaan 200D, B-3001 Leuven, Belgium*

Accepted YYYYMMDD. Received YYYYMMDD; in original form YYYYMMDD.

ABSTRACT

The study of pulsating stars in eclipsing binaries holds the promise of combining two different ways of measuring the physical properties of a star to obtain improved constraints on stellar theory. Gravity (g) mode pulsations such as those found in γ Doradus stars can be used to probe rotational profiles, mixing and magnetic fields. Until recently few γ Doradus stars in eclipsing binaries were known. We have discovered g-mode pulsations in four detached eclipsing binary systems from light curves obtained by the Transiting Exoplanet Survey Satellite (TESS) and present an analysis of their eclipses and pulsational characteristics. We find unresolved g-mode pulsations at frequencies 1–1.5 d^{-1} in CM Lac, and measure the masses and radii of the component stars from the TESS data and published radial velocities. MZ Lac shows a much richer frequency spectrum, including pressure modes and tidally-excited g-modes. RX Dra is in the northern continuous viewing zone of TESS so has a light curve covering a full year, but shows relatively few pulsation frequencies. For V2077 Cyg we formally measure four pulsation frequencies, but the available data are inadequate to properly resolve the g-mode pulsations. V2077 Cyg also shows total eclipses, with which we obtain the first measurement of the surface gravity of the faint secondary star. All four systems are bright and good candidates for detailed study. Further TESS observations are scheduled for all four systems, with much improved temporal baselines in the cases of RX Dra and V2077 Cyg.

Key words: stars: fundamental parameters — stars: binaries: eclipsing — stars: oscillations

1 INTRODUCTION

Eclipsing binary star systems (EBs) are crucial objects for understanding the physics governing stellar structure and evolution, because they are the only stars whose masses and radii can be measured to high precision and accuracy from observational material and geometrical arguments alone. Precise measurements of the masses and radii of stars in EBs were instrumental in the development of stellar theory (e.g. Russell 1914), in the verification of the first modern generation of theoretical stellar models (e.g. Andersen et al. 1990; Pols et al. 1997), and continue to be used to guide theoretical progress (Claret & Torres 2018; Tkachenko et al. 2020). In the current era of échelle spectroscopy and space-based light curves it is possible to measure masses and radii for stars in EB to precisions approaching 0.1% (Maxted et al. 2020; Graczyk et al. 2021). The impact of photometry from space missions has been reviewed in detail by Southworth (2021a).

Another class of stars capable of posing high-quality constraints on stellar theory is that of the pulsating variables (Aerts et al. 2010). Among these, stars showing gravity-mode (g-mode) pulsations are well-suited to studying the interiors of stars as g-modes, which have buoyancy as the dominant restoring force, can travel deep within stars whilst leaving observable signatures on the stellar surface. γ Doradus (γ Dor) variables (Kaye et al. 1999) are stars of types A and F that show g-mode pulsations with periods ranging from 0.3 d to 4 d and amplitudes up to 0.1 mag (Henry et al. 2007; Grigahcène et al. 2010).

In recent years, asteroseismic analyses of main-sequence stars with g-mode pulsations have allowed us to place constraints on multiple phenomena. These include near-core stellar rotation (e.g. Bouabid et al. 2013; Van Reeth et al. 2016; Christophe et al. 2018; Takata et al. 2020a,b; Szewczuk et al. 2021), core boundary mixing (e.g. Michielsen et al. 2019; Wu & Li 2019; Mombarg et al. 2021), extra envelope mixing (e.g. Mombarg et al. 2020; Pedersen et al. 2021) and magnetic fields (e.g. Prat et al. 2019; Van Beeck et al. 2020).

The advantages of asteroseismology and binarity can be combined in objects which show both eclipses and pulsations. These systems have the potential to set exacting constraints on stellar theory (e.g. Johnston et al. 2019b). A wide variety of pulsating stars are known in EBs, including δ Scuti (Maceroni et al. 2014; da Silva et al. 2014; Lee et al. 2020, 2021; Southworth 2021d), β Cephei (Southworth et al. 2020, 2021; Lee & Hong 2021), SPB (Clausen 1996; Southworth & Bowman 2022) and δ Cephei (Pilecki et al. 2018). Over the last decade, multiple γ Dor variables in EBs have been discovered as well. An em-

blematic case is that of KIC 11285625 (Debosscher et al. 2013). Others were found by, among others, Hambleton et al. (2013); Lee et al. (2014); Sowicka et al. (2017); Hełminiak et al. (2017); Guo et al. (2017b); Lampens et al. (2018); Guo et al. (2019) and Van Reeth et al. (2022).

A sample of 115 γ Dor variables in EBs was identified by Gaulme & Guzik (2019) via a systematic search of the *Kepler* EB catalogue (Kirk et al. 2016). Li et al. (2020) performed an asteroseismic evaluation of these targets and reported the detection of g-mode period-spacing patterns for 34 of them, as well as for one discovered by Colman et al. (2021). An independent systematic search and asteroseismic evaluation of the *Kepler* EB catalogue was conducted by Sekaran et al. (2020), resulting in a different sample of 93 γ Dor variables in EBs, with detected period-spacing patterns for seven of them. So far, detailed asteroseismic modelling has only been done for a small number of targets: KIC 10080943 (Schmid & Aerts 2016; Johnston et al. 2019a), KIC 10486425 (Zhang et al. 2018), KIC 7385478 (Guo & Li 2019) and KIC 9850387 (Zhang et al. 2020; Sekaran et al. 2021).

The accumulating data from the NASA Transiting Exoplanet Survey Satellite (TESS; Ricker et al. 2015) is enabling previously unattainable analyses of many of the bright and well-known variable stars. The catalogue of objects includes many EBs with a long observational history (e.g. Southworth 2020). In the course of trawling this database we have discovered four bright EBs whose light curves also show γ Dor pulsations. In this work we present these discoveries, studies of their light and radial velocity (RV) curves, and a first analysis of their asteroseismic nature.

2 OBSERVATIONS

The TESS satellite (Ricker et al. 2015) is in the process of observing almost the entire celestial sphere, split into 69 overlapping sectors. Each sector is a $24^\circ \times 96^\circ$ strip of sky and is photometrically monitored for 27.4 d, through a filter with a high throughput between 600 nm and 1000 nm, with a pause near the midpoint for the download of data to Earth. During the nominal two-year mission, full-frame images (FFI) were taken at a default cadence of 1800 s, while a subset of stars were monitored in short cadence, where successive exposures were combined to yield light curves with a cadence of 120 s. In the ongoing extended mission, the FFI cadence has been changed to 600 s.

Reduced light curves are obtained from the data by the Science Processing Operations Center (SPOC; Jenkins et al. 2016) and made available through the MAST portal[1]. We used the simple amperture photometry (SAP) light curves in the current work. We visually inspected the TESS light curves of approximately 2000 EBs present in a bibliography maintained by the first author, and identified four objects that show both eclipses and previously-unrecognised γ Dor pulsations: CM Lac, MZ Lac, RX Dra and V2077 Cyg.

CM Lac was observed only in sector 16 (2019/09/11 to 2019/10/07) and one further sector of observations is scheduled[2] (sector 56, 2022 September). MZ Lac was observed in two consecutive sectors, 16 and 17 (2019/11 to 2019/11/02) and this will recur in sectors 56–57 (2022 Sept/Oct). By contrast, extensive observations exist for RX Dra because it is sited within the northern continuous viewing zone (CVZ) of TESS. It was observed in sectors 14–26 (2019/07/18 to 2020/07/04) and 40–41 (2021/06/08 to 2021/08/20) and observations are currently being obtained in sectors 47–60 (2021/12/30 to 2023/01/18). V2077 Cyg was observed in sectors 14 (2019/07/18 to 2019/08/15), 26 (2020/06/08 to 2020/07/04) and 41 (2021/07/23 to 2021/08/20), and an additional four consecutive sectors (53–56) will be observed in 2022. The light curves for one sector of each of the four stars are shown in Fig. 1.

Following the target selection, we carefully reassessed the quality of the reduced SAP light curves. First, we inspected the aperture masks used in the pixel data and evaluated both the level of captured flux and the level of contamination from nearby stars. For all stars, the standard SPOC aperture mask was accepted, with the exception of RX Dra. Here, we re-extracted the light curve from the pixel data using custom aperture masks, to account for the varying contamination level between sectors by the nearby non-variable star 2MASS J19024829+5844050. Second, we applied additional detrending to the light curves by fitting low-order polynomials. To avoid overfitting, these detrending curves were optimised simultaneously with preliminary binary and pulsation models, built from a sum of sine waves:

$$f(t) = \sum_{i=1}^{10} a_i \sin\left(2\pi\nu_i\left(t-t_0\right)+\phi_i\right) + \sum_{j=1}^{10} a_j \sin\left(2\pi j\nu_{\rm orb}\left(t-t_0\right)+\phi_j\right)$$

Here, ν_i and $\nu_{\rm orb}$ are estimates for the dominant pulsation frequencies and the orbital frequency, a_i and a_j are their amplitudes, and ϕ_i and ϕ_j are their phases, respectively. The mean timestamp of each light curve was used as the zeropoint t_0.

3 ANALYSIS METHODS

3.1 Light curve analysis

All four systems are well-detached EBs so are suitable for analysis with the JKTEBOP code[3] (Southworth et al. 2004a; Southworth 2013). In this code, the fractional radii of the stars[4] are parameterised as their sum ($r_{\rm A}+r_{\rm B}$) and ratio ($k=\frac{r_{\rm B}}{r_{\rm A}}$), and the orbital eccentricity (e) and argument of periastron are parameterised using the combination terms $e\cos\omega$ and $e\sin\omega$. Other fitted parameters include the orbital period (P), midpoint of primary eclipse (T_0), orbital inclination (i), and the central surface brightness ratio (J). We used the quadratic limb darkening (LD) law, fitted for the linear LD coefficients ($u_{\rm A}$ and $u_{\rm B}$), and fixed the quadratic LD coefficients ($v_{\rm A}$ and $v_{\rm B}$) to theoretical values (Claret 2018). We define the primary eclipse to be the deeper of the two types of eclipse, the primary star (the star eclipsed during primary eclipse) to be star A, and the secondary to be star B.

The presence of pulsations complicates the light curve analysis. In our initial analysis we ignored this and fitted the entire light curve with a JKTEBOP model including one low-order polynomial

[1] https://mast.stsci.edu/portal/Mashup/Clients/Mast/Portal.html
[2] https://heasarc.gsfc.nasa.gov/cgi-bin/tess/webtess/wtv.py
[3] http://www.astro.keele.ac.uk/jkt/codes/jktebop.html
[4] $r_{\rm A}=\frac{R_{\rm A}}{a}$ and $r_{\rm B}=\frac{R_{\rm B}}{a}$ where $R_{\rm A}$ and $R_{\rm B}$ are the true radii and a is the semimajor axis of the relative orbit.

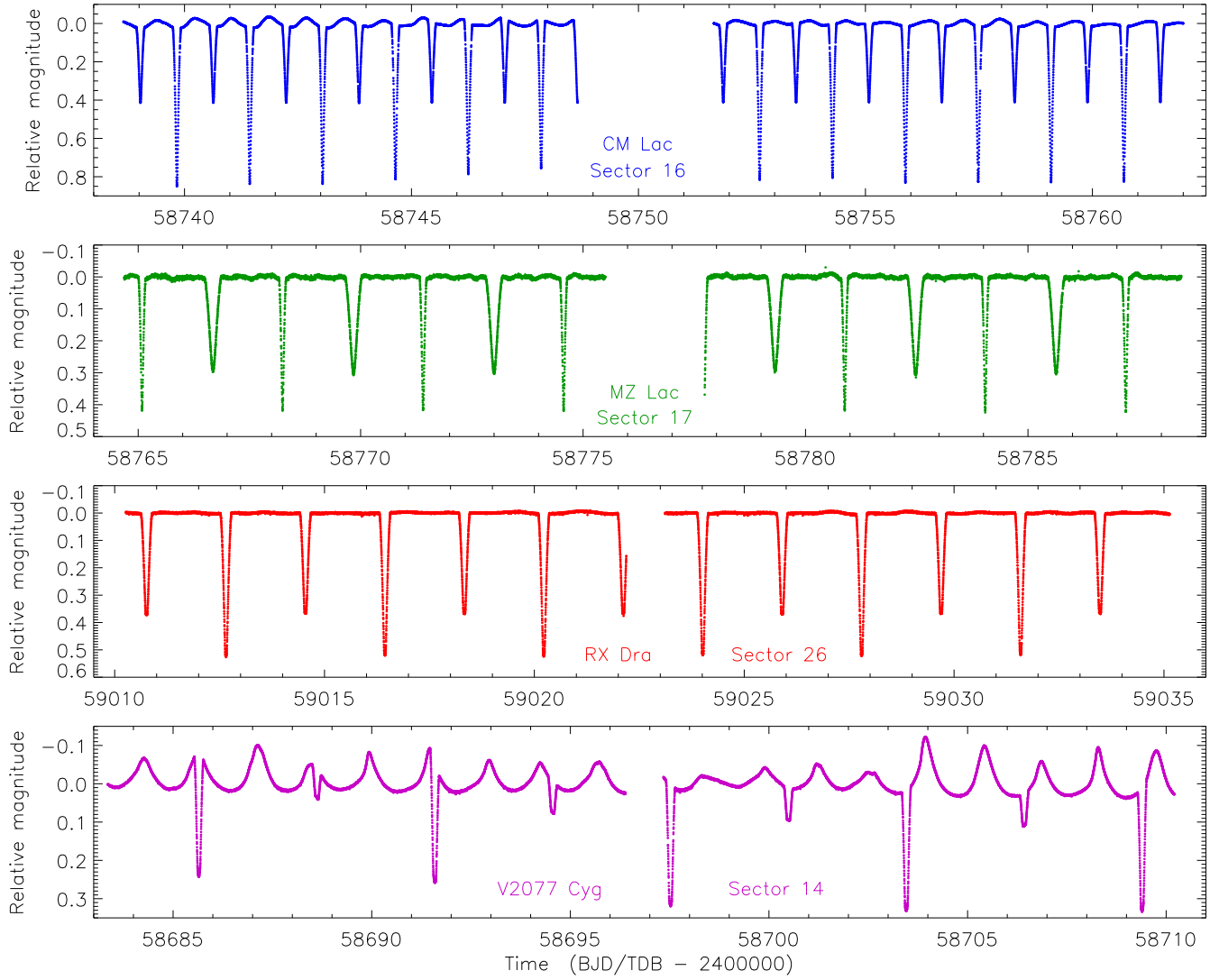

Figure 1. TESS SAP light curves of the four EBs. In each case only one sector is shown.

versus time per TESS half-sector to remove slow drifts in brightness due to instrumental or astrophysical effects. Once the residuals of the fit were obtained, these were subsequently used in the pulsation analysis (see below). For CM Lac and V2077 Cyg we then extracted each eclipse from the data, plus half an eclipse duration either side, and then fitted these together with a low-order polynomial for each eclipse representing the pulsation-induced brightness changes around the time of the eclipse. This procedure was successful in the case of CM Lac, but led to small systematic biases for V2077 Cyg due to the amplitude and complexity of the pulsational signature. For RX Dra the surfeit of data mandated a different approach: an initial fit to the full data followed by phase-binning down into a more manageable number of observations (see Section 4.3).

Uncertainties in the fitted parameters were calculated using the Monte Carlo and residual-permutation simulations implemented in JKTEBOP (Southworth 2008). The Monte Carlo simulations account for correlations between photometric parameters, and required the errorbars in the TESS data to be rescaled to force a reduced χ^2 of $\chi^2_\nu = 1$. The residual-permutation simulations are sensitive to red noise in data, so are useful in the case of unmodelled pulsations. The two errorbars were checked for every parameter and the larger of the two retained in each case. From recent analyses of the TESS light curves of other EBs (Southworth 2021b,c) we have found that the Monte Carlo and residual-permutation simulations typically agree with each other and with errorbars obtained from splitting up light curves into multiple subsets for analysis in isolation. Additional support for the reliability of the Monte Carlo and residual-permutation errorbars, and of the JKTEBOP model, comes from a recent analysis of AI Phe by multiple researchers working independently and using multiple codes and error estimation methods (Maxted et al. 2020). The systematics in the modelling of V2077 Cyg have only a small effect on our results because the system is totally-eclipsing and thus possesses a higher intrinsic determinacy of the photometric parameters (Kopal 1959).

3.2 Pulsation analysis

After a good fit to the light curve had been obtained, the residuals of the fit were calculated and subjected to a frequency analysis. The data points that were obtained during the eclipses were excluded to minimise the influence of any remaining binary signal in the residuals. Because the available TESS data are in most

Table 1. Parameters measured from the eclipses using the JKTEBOP code. Parameters with a superscripted N were calculated using the nominal physical constants and solar quantities defined by the IAU (Prša et al. 2016). The $T_{\rm eff}$ values for CM Lac came from Liakos & Niarchos (2012), and for V2077 Cyg came from Molenda-Żakowicz et al. (2007).

	CM Lac	MZ Lac	RX Dra	V2077 Cyg
Fitted parameters:				
$r_{\rm A} + r_{\rm B}$	0.35383 ± 0.00078	0.2557 ± 0.0024	0.21854 ± 0.000099	0.12303 ± 0.00022
k	0.902 ± 0.018	0.893 ± 0.027	0.7144 ± 0.0010	0.4933 ± 0.0063
i (°)	87.573 ± 0.082	88.53 ± 0.41	88.589 ± 0.018	88.668 ± 0.048
J	0.5956 ± 0.0074	0.888 ± 0.048	0.8063 ± 0.0055	0.321 ± 0.013
L_3	-0.0043 ± 0.0070	0.377 ± 0.018	0.0176 ± 0.0013	-0.026 ± 0.018
$u_{\rm A}$	0.237 ± 0.029	0.62 ± 0.13	0.300 ± 0.031	0.248 ± 0.033
$u_{\rm B}$	0.182 ± 0.040	0.673 ± 0.073	0.195 ± 0.057	0.35 ± 0.11
$v_{\rm A}$	0.232 (fixed)	0.229 (fixed)	0.081 ± 0.050	0.229 (fixed)
$v_{\rm B}$	0.229 (fixed)	0.229 (fixed)	0.316 ± 0.096	0.229 (fixed)
$e \cos \omega$	0.000289 ± 0.000082	0.00732 ± 0.00025	0.000030 ± 0.000010	0.0 fixed
$e \sin \omega$	0.0009 ± 0.0023	0.4116 ± 0.0079	0.00094 ± 0.00062	0.0 fixed
P (d)	1.6046879 ± 0.0000046	3.158794 ± 0.00009	$3.78639491 \pm 0.00000009$	5.937226 ± 0.000068
T_0 (BJD/TDB)	$2458752.67073 \pm 0.00032$	$2458765.08683 \pm 0.00014$	$2458857.410151 \pm 0.000002$	$2458697.52198 \pm 0.00028$
$K_{\rm A}$ (km s^{-1})	120.0 ± 3.4			54.52 ± 0.82
$K_{\rm B}$ (km s^{-1})	157.0 ± 3.3			
$V_{\gamma,{\rm A}}$ (km s^{-1})	22.7 ± 1.9			-0.23 ± 0.40
$V_{\gamma,{\rm B}}$ (km s^{-1})	25.0 ± 1.8			
Derived parameters:				
$r_{\rm A}$	0.1860 ± 0.0015	0.1351 ± 0.0032	0.12747 ± 0.00008	0.08238 ± 0.00038
$r_{\rm B}$	0.1678 ± 0.0021	0.1296 ± 0.0016	0.09107 ± 0.00008	0.04064 ± 0.00034
e	0.0009 ± 0.0015	0.4117 ± 0.0079	0.00094 ± 0.00059	
ω (°)	71^{+213}_{-14}	88.091 ± 0.041	88.2 ± 1.5	
Light ratio	0.495 ± 0.018	0.691 ± 0.062	0.4088 ± 0.0008	0.0750 ± 0.0022
Mass of star A ($\mathcal{M}^{\rm N}_\odot$)	2.01 ± 0.10			
Mass of star B ($\mathcal{M}^{\rm N}_\odot$)	1.54 ± 0.09			
Radius of star A ($\mathcal{R}^{\rm N}_\odot$)	1.636 ± 0.032			
Radius of star B ($\mathcal{R}^{\rm N}_\odot$)	1.476 ± 0.031			
Surface gravity of star A	4.314 ± 0.011			
Surface gravity of star B	4.286 ± 0.016			4.607 ± 0.007
$T_{\rm eff}$ of star A (K)	8700 ± 300 *			7066 ± 201 **
$T_{\rm eff}$ of star B (K)	7034 ± 270 *			

cases limited to one or two sectors per star, which are generally insufficient to resolve individual g-mode pulsations, this remains a preliminary analysis. Using a Lomb-Scargle periodogram (Scargle 1982), we iteratively prewhitened the light curve (Degroote et al. 2009) to measure the pulsations for which the signal-to-noise ratio S/N $\geqslant 4$ (Breger et al. 1993).

The amplitudes, frequencies and phases of these pulsations were subsequently optimised with a non-linear least-squares fit (Bowman 2017) and the S/N ratios were re-evaluated using these optimised parameter values. The derived pulsation frequencies and their combinations were then compared with harmonics of the binary orbital frequency to identify possible tidally excited (e.g., Fuller 2017; Guo et al. 2019), tidally perturbed (e.g., Reyniers & Smeyers 2003; Bowman et al. 2019; Steindl et al. 2021) or non-linearly coupled oscillations (e.g., Burkart et al. 2012; Guo 2020). Combination frequency identifications were accepted if they agreed within 3σ.

Table 2. The parameter values for the significant prewhitened frequency of CM Lac. Bracketed quantities indicate the uncertainty in the final digit of the preceding number.

Frequency (d^{-1})	Amplitude (mmag)	Phase (rad)	S/N
1.1799 (2)	12.5 (1)	0.4276 (12)	6.0

3.3 Physical properties

Published spectroscopic orbits exist for both components of the CM Lac system, allowing us to measure its physical properties directly. To do so we included the published radial velocities (RVs) in the JKTEBOP analysis in order to determine the absolute masses and radii of the stars. In the case of V2077 Cyg RVs are available for the primary but not the secondary component. In this situation the masses and radii of the stars cannot be measured directly (e.g. Hilditch 2001), but it is possible to obtain the surface gravity of the secondary (Southworth et al. 2004b, 2007) and thus verify its evolutionary status. The measured properties of the four targets are given in Table 1, including published effective temperature ($T_{\rm eff}$) values where available.

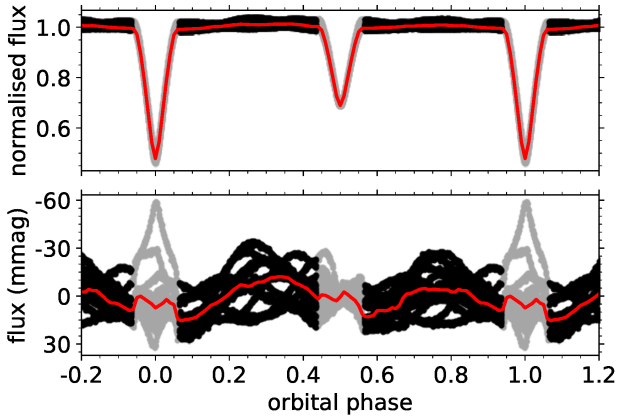

Figure 2. *Top:* TESS light curve of CM Lac (black), phase-folded with the binary period. *Bottom:* Residual light curve of CM Lac after fitting the binary model (black), phase-folded with the binary period. Datapoints taken during the eclipses are marked in grey. For clarity, a binned light curve (with 400 bins) has been overplotted in red in both panels.

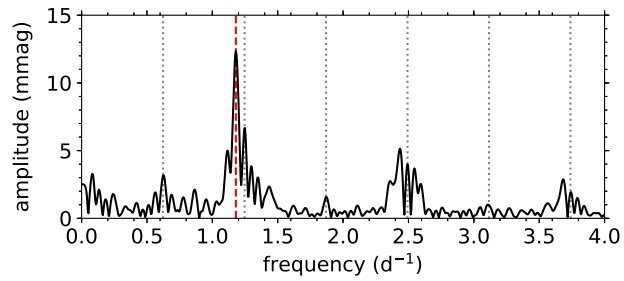

Figure 3. Part of the Lomb-Scargle periodogram (black) of the TESS light curve of CM Lac, excluding the eclipses. The harmonics of the orbital frequency $\nu_{\rm orb}$ (dotted grey lines) and the tentatively extracted pulsation frequency (dashed red line) are also indicated.

4 DISCUSSION OF INDIVIDUAL SYSTEMS

4.1 CM Lacertae

4.1.1 *Analysis of the binary*

CM Lac was discovered to be an eclipsing binary by Wachmann (1931) and physical properties were measured by Popper (1968). The most detailed study of the system was by Liakos & Niarchos (2012), who determined its physical properties based on light curves observed in the $BVRI$ bands and RVs from a set of 28 medium-resolution spectra.

The TESS light curve of CM Lac (Fig. 1) contains 12 primary and 14 secondary eclipses. The pulsations are strong enough to significantly affect the eclipse depths so we cut out the data around each eclipse from the light curve and modelled the out-of-eclipse brightness through each as a quadratic function, as described in Section 3.1. We found that it was possible to constrain one LD coefficient for each star. We also fitted for the amount of third light (L_3), obtaining a slightly negative value. This is physically plausible if the background subtraction in the TESS images is too strong. Although the orbit appears circular, a slight eccentricity is preferred for the TESS data. A phased light curve is shown in Fig. 2.

Our final solution includes the RVs from Liakos & Niarchos (2012) in order to determine the full properties of the system; we fitted for the velocity amplitudes ($K_{\rm A}$ and $K_{\rm B}$) and systemic velocities ($V_{\gamma,{\rm A}}$ and $V_{\gamma,{\rm B}}$) of both stars. The reduced χ^2 of the fit was forced to unity for each dataset by scaling the data errors. We tried including historical times of primary eclipse as well (Wachmann 1931; Kreiner et al. 2001) but they occurred systematically too late so we rejected them – this may suggest that the orbital period of CM Lac is not constant. The uncertainties from residual permutation are larger than those from Monte Carlo. Our results are in Table 1: they agree well with those of Liakos & Niarchos (2012). Further RVs are needed to refine the mass measurements, which are currently precise to only 5%.

4.1.2 *Analysis of the pulsations*

Our frequency analysis reveals the presence of γ Dor pulsations. This can easily be seen from the Fourier transform of the TESS light curve (excluding the eclipses) shown in Fig. 3. There is unresolved variability with frequencies between 1.0 and 1.5 d^{-1}. This is most likely caused by g-mode pulsations, as the (tentative) dominant frequency that can be obtained with iterative prewhitening (listed in Table 2), differs significantly from the harmonics of the binary orbital frequency. However, because the variability is unresolved, the listed frequency value cannot be assigned to a single g-mode pulsation. The asymmetric shape of the light curve is also typical for g-mode pulsations (Kurtz et al. 2015).

We note that the second harmonic of the binary orbital frequency also lies within the frequency range of the observed variability, as shown in Fig. 3. However, because the available TESS data only cover 27 d, we cannot investigate the nature of the variability at this frequency. It may be caused by unresolved nearby g-mode pulsation frequencies, tidally excited or tidally perturbed pulsations, or a residual signature of the binarity. More high-precision photometric data are needed to resolve this issue. From a visual inspection of the TESS light curve, we find that the pulsations remain visible during the primary eclipse, but vanish during the secondary eclipse. This means that the g-mode pulsations belong to the secondary star.

4.2 MZ Lacertae

4.2.1 *Analysis of the binarity*

MZ Lac was found to be an EB by Miller & Wachmann (1971), where it is labelled VV 399, but has been the subject of very little study since. It exhibits apsidal motion (Silhan 1990) with a period of 424 ± 6 yr (Bulut et al. 2016). The TESS light curve shows deep eclipses (Fig. 1) and covers two sectors. The secondary eclipse is at approximately phase 0.5 but is significantly longer than the primary, so $e \cos \omega \approx 0$ but $e \sin \omega$ is large.

The pulsations in MZ Lac have a much lower amplitude than the eclipses so we treated them as red noise: we fitted the whole dataset with JKTEBOP without attempting to reject out-of-eclipse data or compensate for the pulsations in any way. We fitted for the same parameters as for CM Lac, except for those related to RVs and for the inclusion of only four polynomials for the out-of-eclipse brightness of the system. Due to the apsidal motion we did not attempt to use published eclipse timings to help constrain the orbital ephemeris. A substantial amount of third light is required to obtain a good fit to the data.

We were able to find a good fit to the light curve (Table 1). The residual-permutation errorbars are significantly larger than the Monte Carlo errorbars, which suggests it would be possible to improve the light curve analysis in future by either subtracting the pul-

Table 3. An overview of the parameter values for the significant frequencies of MZ Lac. For frequencies that lie close to harmonics of the binary orbital frequency $\nu_{\rm orb}$, the differences between those frequencies and their corresponding harmonics are also given. Possible combination frequencies are listed in the last column.

	Frequency (d^{-1})	Amplitude (mmag)	Phase (rad)	S/N	i	$i\nu_{\rm orb} - \nu$	Comments
ν_1	0.31523 (14)	1.66 (3)	0.495 (2)	12.3	1	−0.00135 (14)	
ν_2	0.8729 (4)	0.70 (2)	−0.477 (5)	5.9			
ν_3	1.2665 (2)	1.46 (3)	0.131 (3)	14.7	4	0.0002 (2)	
ν_4	1.5819 (4)	0.60 (3)	−0.103 (7)	6.3	5	−0.0010 (4)	
ν_5	1.6094 (3)	0.74 (2)	−0.326 (5)	7.9			
ν_6	1.73674 (14)	1.86 (2)	0.424 (2)	20.5			$2\nu_2 + \nu_6 = 11.000(3)\,\nu_{\rm orb}$
ν_7	1.8991 (4)	0.74 (3)	−0.441 (5)	8.2	6	−0.0004 (4)	
ν_8	2.1884 (2)	1.13 (2)	0.038 (3)	14.2			$\nu_5 + \nu_8 = 11.9966(12)\,\nu_{\rm orb}$
ν_9	2.9357 (3)	0.85 (2)	−0.458 (4)	12.8			$\nu_2 + \nu_9 = 12.0303(16)\,\nu_{\rm orb}$
ν_{10}	3.79908 (14)	1.81 (2)	0.424 (2)	32.5	12	0.0002 (2)	
ν_{11}	46.6367 (7)	0.33 (2)	0.264 (11)	13.0			
ν_{12}	48.362 (2)	0.14 (2)	−0.20 (3)	4.4			
ν_{13}	49.1942 (9)	0.26 (2)	−0.408 (14)	8.4			
ν_{14}	51.2559 (4)	0.57 (2)	−0.334 (7)	20.3			

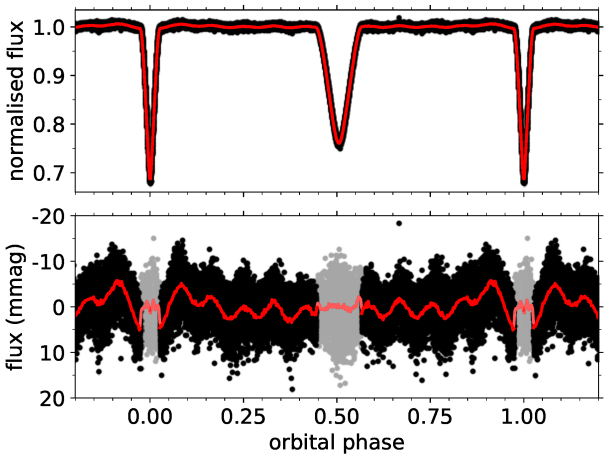

Figure 4. *Top:* TESS light curve of MZ Lac (black), phase-folded with the binary period. *Bottom:* Residual light curve of MZ Lac after fitting the binary model (black), phase-folded with the binary period. Datapoints taken during the eclipses are marked in grey. For clarity, the binned light curve (with 400 bins) has been overplotted in red in both panels.

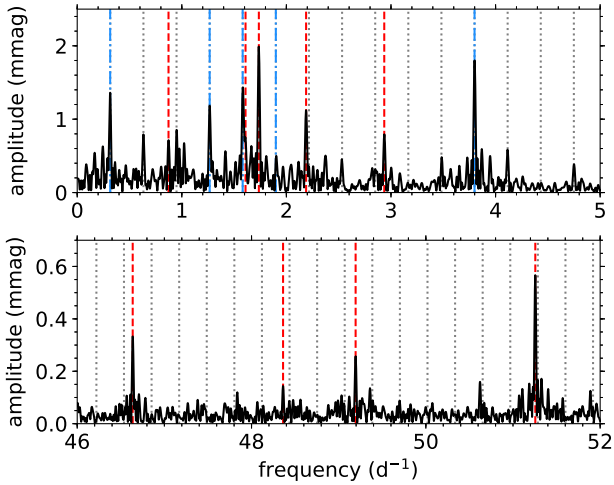

Figure 5. Sections of the Lomb-Scargle periodogram (black) of the residual light curve of MZ Lac (shown in the bottom part of Fig. 4). The harmonics of the orbital frequency $\nu_{\rm orb}$ (dotted grey lines) and the extracted pulsation frequencies are also indicated. The dashed red lines and dash-dotted blue lines mark non-harmonic and harmonic pulsation frequencies, respectively.

sations or fitting for them simultaneously. The full physical properties of the system cannot be calculated as no RVs are available. *Gaia* DR2 (Gaia Collaboration et al. 2018) gives a $T_{\rm eff}$ of the system of 6900 K; if this is appropriate for star A then the $T_{\rm eff}$ of star B is 6700 K based on the value of J we measure. These values are consistent with the presence of δ Sct and γ Dor pulsations (Grigahcène et al. 2010; Murphy et al. 2019).

4.2.2 *Analysis of the pulsations*

From a detailed analysis of the TESS photometry, we find that MZ Lac exhibits an interesting variety of pulsation behaviour. Following the binary modelling, we excluded the eclipses from the residual light curve (as indicated in Fig. 4) and used this clipped light curve for the iterative prewhitening. The prewhitened pulsation frequencies of MZ Lac are listed in Table 3 and shown in Fig. 5.

Ten frequencies below $5\,\mathrm{d}^{-1}$ have been measured from the TESS light curve. Five of these lie significantly close to harmonics of the orbital frequency, and four are well within 3σ. A visual inspection of the light curve, phase-folded with the binary orbital period as shown in Fig. 4, reveals that these frequencies are likely related to tidally excited pulsations. While an imperfect fit of the binary orbit to the light curve might cause a similar signal in the Fourier domain, the dominant variation seen in the phase-folded light curve (in Fig. 4) occurs on a shorter timescale than would be expected in this case.

We also obtain five non-harmonic low frequencies. While these have values of typical γ Dor-type pulsations, three pairs of them form combination frequencies that (almost) coincide with harmonics of the orbital frequency: $2\nu_2 + \nu_6 = 11.000(3)\,\nu_{\rm orb}$, $\nu_5 + \nu_8 = 11.9966(12)\,\nu_{\rm orb}$ and $\nu_2 + \nu_9 = 12.0303(16)\,\nu_{\rm orb}$. The first two combinations match the closest orbital harmonics within 3σ, and the last one matches the orbital harmonic within $\nu_{\rm res}$. This can be caused by nonlinear mode coupling, whereby the orbital harmonic is the parent frequency and the observed non-harmonic frequencies are the child frequencies (e.g., Burkart et al.

Table 4. An overview of the parameter values for the significant frequencies of RX Dra. Possible combination frequencies within 3σ are also listed.

	Frequency (d^{-1})	Amplitude (mmag)	Phase (rad)	S/N	Combinations
ν_1	0.40386 (2)	0.407 (5)	0.104 (2)	9.4	
ν_2	0.48268 (1)	0.64 (5)	−0.486 (1)	15.2	
ν_3	0.51792 (3)	0.252 (5)	−0.484 (3)	6.0	$\nu_{19} - \nu_{11}$
ν_4	0.54059 (2)	0.376 (5)	0.296 (2)	9.1	
ν_5	0.56659 (2)	0.516 (5)	0.492 (2)	12.5	
ν_6	0.58234 (2)	0.395 (5)	0.371 (2)	9.6	
ν_7	0.63871 (2)	0.41 (5)	0.235 (2)	10.1	
ν_8	0.65485 (2)	0.373 (5)	0.491 (2)	9.2	$\nu_{17} - \nu_2$
ν_9	0.69392 (1)	0.596 (5)	0.204 (1)	14.8	$\nu_{18} - \nu_2$
ν_{10}	0.72459 (4)	0.224 (5)	0.401 (4)	5.6	$\nu_{20} - \nu_6$
ν_{11}	0.75959 (1)	0.674 (5)	−0.414 (1)	17.0	
ν_{12}	0.77293 (2)	0.397 (5)	−0.096 (2)	10.0	
ν_{13}	0.81678 (2)	0.365 (5)	0.391 (2)	9.3	
ν_{14}	0.91214 (2)	0.526 (5)	−0.26 (2)	13.8	
ν_{15}	0.92597 (2)	0.393 (5)	0.115 (2)	10.4	
ν_{16}	1.10811 (5)	0.179 (5)	−0.442 (5)	5.0	
ν_{17}	1.13749 (2)	0.466 (5)	0.479 (2)	13.2	
ν_{18}	1.176625 (6)	1.405 (5)	−0.2303 (6)	41.0	
ν_{19}	1.27764 (3)	0.276 (5)	0.265 (3)	8.5	
ν_{20}	1.30693 (3)	0.274 (5)	−0.002 (3)	8.6	
ν_{21}	1.5985 (6)	0.132 (5)	−0.03 (6)	5.1	
ν_{22}	1.71749 (4)	0.187 (5)	0.324 (4)	7.7	
ν_{23}	1.74289 (3)	0.289 (5)	−0.44 (3)	12.1	
ν_{24}	2.8467 (1)	0.054 (5)	0.37 (1)	4.3	

2012; Weinberg et al. 2013; Guo et al. 2017a). Finally, there are four pressure-mode (p-mode) pulsations, with frequencies between 46 and 51.5 d^{-1}.

From a visual inspection of the TESS light curve shown in Fig.4, we find that the pulsations (as illustrated in the bottom panel of Fig.4) appear to be less visible during *both* eclipses. Our best explanation for this apparent physical inconsistency is that the (tidally excited) pulsations were partially fitted by the binary model in the eclipses. This could have happened in particular if the pulsations had a similar effect on the eclipse shape as LD, as some LD coefficients were included as fitted parameters. The fitted LD coefficients are indeed larger than expected. Whilst one approach to fixing this problem might be to fix the LD coefficients, this risks biasing the measured radii because theoretical LD coefficients are not completely reliable. An alternative approach in future could be to simultaneously model the eclipses and the pulsations.

4.3 RX Draconis

4.3.1 Analysis of the binarity

RX Dra has been known to be eclipsing for over a century. The first photometric analysis was given by Shapley (1913) but it has received very little attention subsequently. It came to the authors' attention by its inclusion in a list of EBs that are candidates for hosting pulsating stars (Soydugan et al. 2006), and inspection of its TESS light curve revealed clear pulsations of the γ Dor type. TESS observations are available for 13 consecutive sectors (14–26) followed by two further sectors (40 and 41). At the time of writing, observations are also ongoing for 14 consecutive sectors (47–60); see Section 2. We base our results in the current work on the data from sectors 14–26.

Because of the huge amount of data (230 766 observations sampled at 120 s cadence for one year) covering a large number of eclipses (approximately 170) we first obtained a preliminary solution with JKTEBOP to establish the orbital ephemeris. We then converted the data into orbital phase and binned them into 1000 points equally spaced in phase. The primary eclipse is annular and the secondary eclipse is total. A good fit to the binned data can be obtained comparatively easily due to the total eclipses. We included orbital eccentricity and third light as fitted parameters and both come out at very small but probably non-zero. It was also possible to fit for *both* LD coefficients for both stars, an occurrence the first author has not previously encountered despite having recently studied the TESS light curves of over 50 EBs. The errorbars from the Monte Carlo algorithm were adopted as they are significantly larger than those from the residual-permutation approach. Our results are given in Table 1. The uncertainties in the fractional radii are below 0.1%, but we recommend that interested users increase them to at least 0.1% as this is the lower limit of reliability established by comparing independent analyses of the same data for a similar EB (Maxted et al. 2020).

4.3.2 Analysis of the pulsations

RX Dra is an outlier in our sample. While we only have one or two TESS sectors of data available for most of our stars, RX Dra is located in the northern CVZ and has been observed during 13 consecutive sectors sectors, spanning 351 days in total. This has allowed us to better resolve the individual stellar pulsation frequencies and measure them with a higher precision, as listed in Table 4 and shown in Fig. 6.

Despite the short orbital period, all observed pulsations were found to be intrinsic g-mode pulsations. Four of the 24 measured frequencies form combinations within 3σ. Additionally, the observed pulsation spectrum is relatively sparse, given that we have almost a full year of photometry at our disposal. The inclusion of additional photometric observations, such as those that are currently being taken during TESS cycle 4, may improve the window functions of the stellar pulsations sufficiently to allow us to measure more g-mode pulsation frequencies.

Similarly to the pulsations observed for MZ Lac, we cannot assign the pulsations of RX Dra to a specific component. Here, the narrow triangular shapes of the eclipses do not suffice to evaluate the pulsation amplitudes as a function of the light contribution of the individual components, as illustrated in Fig. 7. Additionally, the measured g-mode frequencies are too sparse to detect clear g-mode period-spacing patterns, which would have allowed us to perform pulsation mode identification and select a group or groups of pulsations that originate from the same stellar component in the binary system. There is, however, clear structure present in the observed g-mode pulsation spectrum. The inclusion of the forthcoming TESS observations will be needed to detect period-spacing patterns for RX Dra if they are present in the data.

4.4 V2077 Cygni

4.4.1 Analysis of the binarity

V2077 Cyg was identified as an EB using photometry from the *Hipparcos* satellite, and given its GCVS designation by Kazarovets et al. (1999) as a result. The only study of the object so far was performed by Molenda-Żakowicz et al. (2007), who obtained 29 spectra and measured the spectroscopic orbit of the primary star. The secondary is much fainter and was not detected

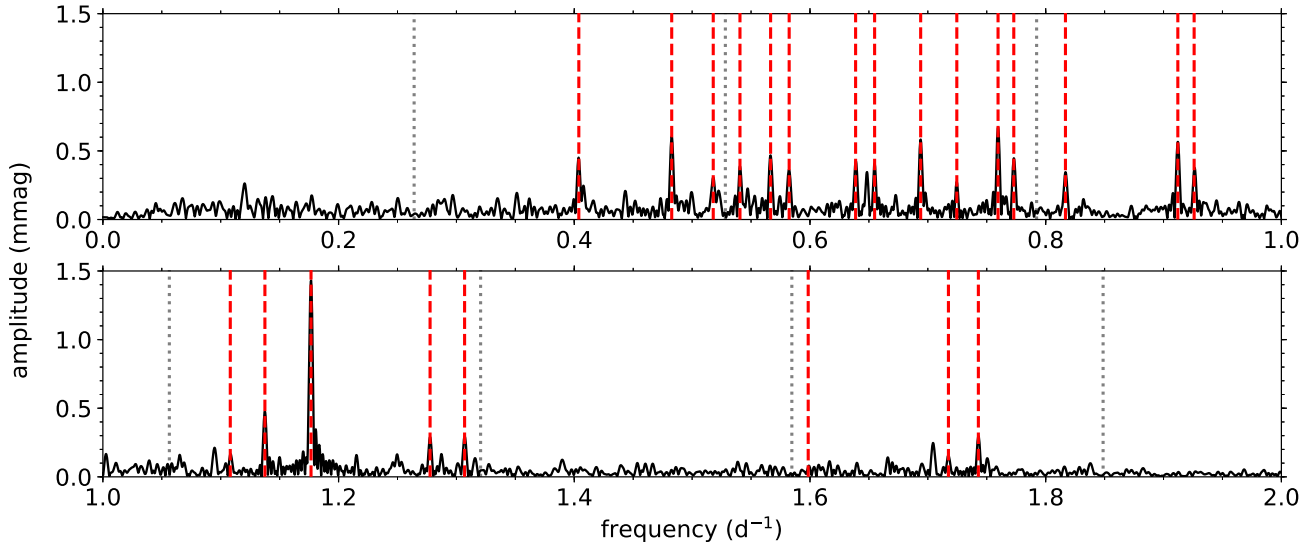

Figure 6. Sections of the Lomb-Scargle periodogram (black) of the residual light curve of RX Dra (shown in the bottom part of Fig. 7). The harmonics of the orbital frequency $\nu_{\rm orb}$ (dotted grey lines) and the extracted pulsation frequencies (dashed red lines)are also indicated.

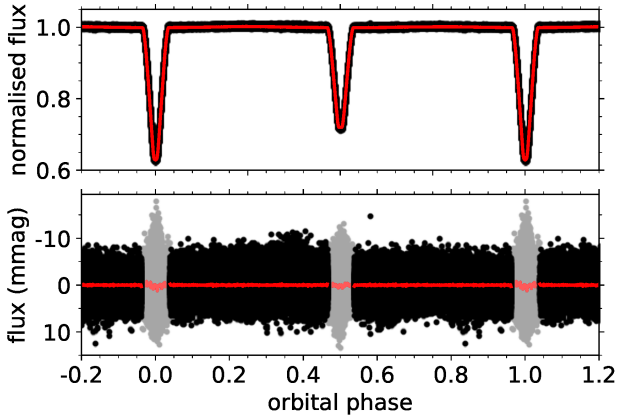

Figure 7. *Top:* The TESS light curve of RX Dra (black), phase-folded with the binary period. For clarity, the binned light curve (with 400 bins) has been overplotted in red. *Bottom:* The residual light curve of RX Dra after subtracting the binary signal (grey) and excluding the time stamps of the eclipses (black), phase-folded with the binary period. For clarity, the binned light curve (with 400 bins) has again been overplotted in red.

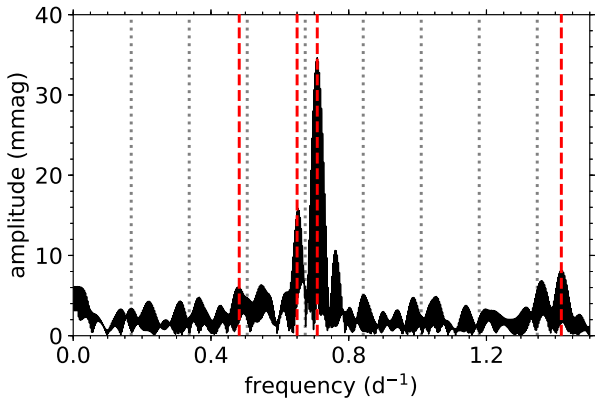

Figure 8. Part of the Lomb-Scargle periodogram (black) of the residual light curve of V2077 Cyg (after the best-fitting binary model has been subtracted). The harmonics of the orbital frequency $\nu_{\rm orb}$ (dashed grey lines) and the extracted pulsation frequencies (dashed red lines) are also indicated.

Table 5. An overview of the parameter values for the significant frequencies of V2077 Cyg. The identification of possible combination frequencies within 3σ is also given.

	Frequency (d^{-1})	Amplitude (mmag)	Phase (rad)	S/N	Combinations
ν_1	0.48209 (1)	6.97 (10)	−0.244 (2)	4.1	
ν_2	0.65013 (1)	8.5 (1)	−0.163 (2)	5.3	
ν_3	0.708696 (3)	33.4 (1)	0.4049 (5)	21.1	
ν_4	1.41741 (1)	8.72 (10)	0.075 (2)	6.7	$\nu_4 \approx 2\nu_3$

in the spectra. The TESS light curve (Fig. 1) shows distinctive saw-toothed pulsations characteristic of γ Dor pulsators, plus primary eclipses that are much deeper than the secondary eclipses. The light curve is strongly reminiscent of the prototypical system KIC 11285625 (Debosscher et al. 2013), except that the eclipses are total. TESS has observed the star during three sectors (14, 26 and 41) and four further sectors of observations (53, 54, 55 and 56) are planned. The four consecutive sectors will be valuable for increasing the precision of the measured pulsation periods. The following analyses only includes sectors 14 and 26, as sector 41 was not available at the time they were performed.

The pulsation amplitudes are comparable to the eclipse depths so we proceeded as for CM Lac (Sect. 4.1): each eclipse was extracted from the light curve and normalised to zero differential magnitude using a polynomial function. We found that a third-order polynomial was necessary in some cases. The light curve was then fitted as for CM Lac, with the exception that we had RVs for only the primary star so did not fit for $K_{\rm B}$ or $V_{\gamma,{\rm B}}$. The results are given in Table 1. The fractional radii of the stars are well-measured because of the presence of total eclipses in this system.

Molenda-Żakowicz et al. (2007) measured a $T_{\rm eff}$ of 7066 ± 201 K for the primary star, in good agreement with the *Gaia* DR2

value of 6900 K. Our value of J then implies a $T_{\rm eff}$ of 5200 K for the secondary star. Using equation 4 from Southworth et al. (2007) we determine the surface gravity of the secondary star to be $\log g_{\rm B} = 4.607 \pm 0.007$, which is appropriate for a K-dwarf. The γ Dor pulsations arise in the primary component: the secondary is too cool to be a γ Dor star and it also does not contribute enough light to the system to produce pulsations with an amplitude of 0.1 mag.

4.4.2 *Analysis of the pulsations*

Four significant frequencies, listed in Table 5 and illustrated in Fig. 8, can be obtained from iterative prewhitening of the residual TESS light curve. The derived parameter values for these frequencies are all consistent with those expected for γ Dor-type pulsations. However, the available TESS data are again insufficient to ensure that the individual g-mode pulsation frequencies are properly resolved.

More TESS data are needed to properly identify the individual pulsations in this system. Fortunately, it is scheduled to be observed in four consecutive sectors (53–56). If TESS continues to operate as expected, V2077 Cyg will be a useful system for the study of pulsations in a star of known mass and radius.

5 SUMMARY AND CONCLUSIONS

The study of pulsating stars in EBs is a promising opportunity to improve our understanding of the interior physics of stars. Gravity-mode pulsations are a high priority because they can probe regions deep inside a star and thus help constrain stellar rotation, core boundary mixing, envelope mixing, opacity and magnetic fields (see references in Section 1). In pursuit of this goal we have surveyed the TESS light curves of a sample of known EBs and detected g-mode pulsations in four of these. In this work we present a preliminary analysis of all four systems.

CM Lac shows very deep eclipses (0.8 mag for the primary and 0.4 mag for the secondary) and unresolved g-modes with frequencies between $1\,{\rm d}^{-1}$ and $1.5\,{\rm d}^{-1}$ in the one sector of available TESS data. The available data are therefore insufficient for asteroseismology, but remain useful for the determination of the physical properties of stars. We measured the masses and radii of the component stars using the TESS data and the results of a published RV study, but additional RVs are needed to measure their masses to the canonical 2% precision (Andersen 1991).

MZ Lac is a more interesting system due to its large orbital eccentricity (Table 1) and richer pulsation spectrum. Based on the two sectors of TESS data for this object we found evidence for p-modes and for tidally excited or tidally perturbed g-mode pulsations. No RVs are currently available for this object so we are not yet able to determine its physical properties.

RX Dra has been observed for 13 consecutive sectors by TESS but this abundance of data yielded only relatively few identified frequencies. The presence of total eclipses allowed the fractional radii of the stars to be measured to exceptional precision so the system is a good candidate for precise measurement of its physical properties. RX Dra is in the process of being observed for a further 14 consecutive sectors by TESS and these additional data may allow the detection of further pulsation frequencies.

V2077 Cyg shows beautiful γ Dor pulsations but the few currently-available TESS light curves are insufficient to perform mode identification. The system is scheduled for observation in three consecutive sectors by TESS in 2022 and these new data should greatly improve the asteroseismic potential of this system. V2077 Cyg is not promising from the viewpoint of determining its physical properties for two reasons. The eclipses are perturbed by the high-amplitude g-mode pulsations, but are total so precise fractional radii are still measurable. The secondary star is much fainter than the primary (light ratio of 0.075 in the TESS passband) so measuring its RVs will require high-quality spectroscopy. A single-lined spectroscopic orbit exists for this system, allowing us to measure the surface gravity of the secondary component and verify that it is a normal low-mass main-sequence star.

All four systems need detailed spectroscopic study to measure their physical properties precisely, which in turn provides context for the pulsation analysis. This work has begun.

DATA AVAILABILITY

All data underlying this article are available in the MAST archive (https://mast.stsci.edu/portal/Mashup/Clients/Mast/Portal.html).

ACKNOWLEDGEMENTS

TVR gratefully acknowledges support from the Research Foundation Flanders (FWO) under grant agreement N°12ZB620N. We thank Johanna Molenda-Żakowicz for sending us her RV measurements for V2077 Cyg. The TESS data presented in this paper were obtained from the Mikulski Archive for Space Telescopes (MAST) at the Space Telescope Science Institute (STScI). STScI is operated by the Association of Universities for Research in Astronomy, Inc., under NASA contract NAS5-26555. Support to MAST for these data is provided by the NASA Office of Space Science via grant NAG5-7584 and by other grants and contracts. Funding for the TESS mission is provided by the NASA Explorer Program. This research has made use of the SIMBAD database, operated at CDS, Strasbourg, France; the SAO/NASA Astrophysics Data System; and the VizieR catalogue access tool, CDS, Strasbourg, France.

REFERENCES

Aerts C., Christensen-Dalsgaard J., Kurtz D. W., 2010, Asteroseismology. Astron. and Astroph. Library, Springer Netherlands, Amsterdam
Andersen J., 1991, A&ARv, 3, 91
Andersen J., Clausen J. V., Nordström B., 1990, ApJ, 363, L33
Bouabid M. P., Dupret M. A., Salmon S., Montalbán J., Miglio A., Noels A., 2013, MNRAS, 429, 2500
Bowman D. M., 2017, Amplitude modulation of pulsation modes in delta Scuti stars. Springer Theses series, Springer, US
Bowman D. M., Johnston C., Tkachenko A., Mkrtichian D. E., Gunsriwiwat K., Aerts C., 2019, ApJ, 883, L26
Breger M., et al., 1993, A&A, 271, 482
Bulut A., Bulut I., Çiçek C., Erdem A., 2016, in American Institute of Physics Conference Series. p. 040002
Burkart J., Quataert E., Arras P., Weinberg N. N., 2012, MNRAS, 421, 983
Christophe S., Ballot J., Ouazzani R. M., Antoci V., Salmon S. J. A. J., 2018, A&A, 618, A47
Claret A., 2018, A&A, 618, A20
Claret A., Torres G., 2018, ApJ, 859, 100
Clausen J. V., 1996, A&A, 308, 151
Colman I. L., Bedding T. R., Huber D., Kjeldsen H., 2021, ApJS, in press, arXiv:2112.05174
Debosscher J., et al., 2013, A&A, 556, A56
Degroote P., et al., 2009, A&A, 506, 111

Fuller J., 2017, MNRAS, 472, 1538
Gaia Collaboration et al., 2018, A&A, 616, A1
Gaulme P., Guzik J. A., 2019, A&A, 630, A106
Graczyk D., et al., 2021, A&A, 649, A109
Grigahcène A., et al., 2010, ApJ, 713, L192
Guo Z., 2020, ApJ, 896, 161
Guo Z., Li G., 2019, ApJ, 882, L5
Guo Z., Gies D. R., Fuller J., 2017a, ApJ, 834, 59
Guo Z., Gies D. R., Matson R. A., 2017b, ApJ, 851, 39
Guo Z., Fuller J., Shporer A., Li G., Hambleton K., Manuel J., Murphy S., Isaacson H., 2019, ApJ, 885, 46
Hambleton K. M., et al., 2013, MNRAS, 434, 925
Hełminiak K. G., Ukita N., Kambe E., Kozłowski S. K., Pawłaszek R., Maehara H., Baranec C., Konacki M., 2017, A&A, 602, A30
Henry G. W., Fekel F. C., Henry S. M., 2007, AJ, 133, 1421
Hilditch R. W., 2001, An Introduction to Close Binary Stars. Cambridge University Press, Cambridge, UK
Jenkins J. M., et al., 2016, in Proc. SPIE. p. 99133E
Johnston C., Tkachenko A., Aerts C., Molenberghs G., Bowman D. M., Pedersen M. G., Buysschaert B., Pápics P. I., 2019a, MNRAS, 482, 1231
Johnston C., Pavlovski K., Tkachenko A., 2019b, A&A, 628, A25
Kaye A. B., Handler G., Krisciunas K., Poretti E., Zerbi F. M., 1999, PASP, 111, 840
Kazarovets E. V., Samus N. N., Durlevich O. V., Frolov M. S., Antipin S. V., Kireeva N. N., Pastukhova E. N., 1999, Information Bulletin on Variable Stars, 4659, 1
Kirk B., et al., 2016, AJ, 151, 68
Kopal Z., 1959, Close binary systems. The International Astrophysics Series, London: Chapman & Hall
Kreiner J. M., Kim C.-H., Nha I.-S., 2001, An atlas of O-C diagrams of eclipsing binary stars
Kurtz D. W., Shibahashi H., Murphy S. J., Bedding T. R., Bowman D. M., 2015, MNRAS, 450, 3015
Lampens P., et al., 2018, A&A, 610, A17
Lee J. W., Hong K., 2021, AJ, 161, 32
Lee J. W., Kim S.-L., Hong K., Lee C.-U., Koo J.-R., 2014, AJ, 148, 37
Lee J. W., Hong K., Kristiansen M. H., 2020, PASJ, 72, 37
Lee J. W., Hong K., Kim H.-Y., 2021, AJ, 161, 129
Li G., Guo Z., Fuller J., Bedding T. R., Murphy S. J., Colman I. L., Hey D. R., 2020, MNRAS, 497, 4363
Liakos A., Niarchos P., 2012, Ap&SS, 340, 281
Maceroni C., et al., 2014, A&A, 563, A59
Maxted P. F. L., et al., 2020, MNRAS, 498, 332
Michielsen M., Pedersen M. G., Augustson K. C., Mathis S., Aerts C., 2019, A&A, 628, A76
Miller W. J., Wachmann A. A., 1971, Ricerche Astronomiche, 8, 12
Molenda-Żakowicz J., Frasca A., Latham D. W., Jerzykiewicz M., 2007, AcA, 57, 301
Mombarg J. S. G., Dotter A., Van Reeth T., Tkachenko A., Gebruers S., Aerts C., 2020, ApJ, 895, 51
Mombarg J. S. G., Van Reeth T., Aerts C., 2021, A&A, 650, A58
Murphy S. J., Hey D., Van Reeth T., Bedding T. R., 2019, MNRAS, 485, 2380
Pedersen M. G., et al., 2021, Nature Astronomy, 5, 715
Pilecki B., et al., 2018, ApJ, 862, 43
Pols O. R., Tout C. A., Schroder K.-P., Eggleton P. P., Manners J., 1997, MNRAS, 289, 869
Popper D. M., 1968, ApJ, 154, 191
Prat V., Mathis S., Buysschaert B., Van Beeck J., Bowman D. M., Aerts C., Neiner C., 2019, A&A, 627, A64
Prša A., et al., 2016, AJ, 152, 41
Reyniers K., Smeyers P., 2003, A&A, 404, 1051
Ricker G. R., et al., 2015, Journal of Astronomical Telescopes, Instruments, and Systems, 1, 014003
Russell H. N., 1914, The Observatory, 37, 165
Scargle J. D., 1982, ApJ, 263, 835
Schmid V. S., Aerts C., 2016, A&A, 592, A116
Sekaran S., et al., 2020, A&A, 643, A162
Sekaran S., Tkachenko A., Johnston C., Aerts C., 2021, A&A, 648, A91
Shapley H., 1913, ApJ, 38, 158
Silhan J., 1990, JAAVSO, 19, 12
Southworth J., 2008, MNRAS, 386, 1644
Southworth J., 2013, A&A, 557, A119
Southworth J., 2020, The Observatory, 140, 247
Southworth J., 2021a, Universe, 7, 369
Southworth J., 2021b, The Observatory, 141, 122
Southworth J., 2021c, The Observatory, 141, 190
Southworth J., 2021d, The Observatory, 141, 282
Southworth J., Bowman D. M., 2022, MNRAS, submitted
Southworth J., Maxted P. F. L., Smalley B., 2004a, MNRAS, 351, 1277
Southworth J., Zucker S., Maxted P. F. L., Smalley B., 2004b, MNRAS, 355, 986
Southworth J., Wheatley P. J., Sams G., 2007, MNRAS, 379, L11
Southworth J., Bowman D., Tkachenko A., Pavlovski K., 2020, MNRAS, 497, L19
Southworth J., Bowman D. M., Pavlovski K., 2021, MNRAS, 501, L65
Sowicka P., Handler G., Dębski B., Jones D., Van de Sande M., Pápics P. I., 2017, MNRAS, 467, 4663
Soydugan E., Soydugan F., Demircan O., İbanoğlu C., 2006, MNRAS, 370, 2013
Steindl T., Zwintz K., Bowman D. M., 2021, A&A, 645, A119
Szewczuk W., Walczak P., Daszyńska-Daszkiewicz J., 2021, MNRAS, 503, 5894
Takata M., Ouazzani R. M., Saio H., Christophe S., Ballot J., Antoci V., Salmon S. J. A. J., Hijikawa K., 2020a, A&A, 635, A106
Takata M., Ouazzani R. M., Saio H., Christophe S., Ballot J., Antoci V., Salmon S. J. A. J., 2020b, A&A, 644, A138
Tkachenko A., et al., 2020, A&A, 637, A60
Van Beeck J., Prat V., Van Reeth T., Mathis S., Bowman D. M., Neiner C., Aerts C., 2020, A&A, 638, A149
Van Reeth T., Tkachenko A., Aerts C., 2016, A&A, 593, A120
Van Reeth T., Southworth J., Van Beeck J., Bowman D. M., 2022, A&A, 659, A177
Wachmann A. A., 1931, AN, 244, 303
Weinberg N. N., Arras P., Burkart J., 2013, ApJ, 769, 121
Wu T., Li Y., 2019, ApJ, 881, 86
Zhang X. B., Fu J. N., Luo C. Q., Ren A. B., Yan Z. Z., 2018, ApJ, 865, 115
Zhang X., Chen X., Zhang H., Fu J., Li Y., 2020, ApJ, 895, 124
da Silva R., Maceroni C., Gandolfi D., Lehmann H., Hatzes A. P., 2014, A&A, 565, A55

This paper has been typeset from a TEX/LATEX file prepared by the author.